

Recent Progress in Calibration of the RXTE Proportional Counter Array

Keith Jahoda and the PCA Team

GSFC Laboratory for High Energy Astrophysics

13 January 1997, 189th AAS meeting

This poster concentrates on the status of the Proportional Counter Array energy response matrix. Examples are given for data from the Crab nebula plus pulsar.

Current information on the calibration of the PCA can be found at

<http://lheawww.gsfc.nasa.gov/docs/xray/xte/pca> .

1 Elements of the Response Matrix

We identify three separable tasks which must be performed in order to create a response matrix. These are to

- (a) determine the energy to channel conversion. By this we mean what is the mean channel in which X-rays of a particular energy will be detected. This determination ignores X-rays detected in escape peaks, which are treated in (c)).
- (b) estimate the quantum efficiency with which photons of a given energy are detected; and
- (c) estimate the response in channel space to monochromatic input for a range of energies.

This poster gives the status of each of these 3 tasks and examples of our results.

2 Energy to Channel Conversion

Each of the 5 Proportional Counter Units is continuously illuminated by an Am^{241} source which produces tagged calibration photons at energies between 13 and 60 keV. Occasionally, data is also collected which includes the α flag and 2 lower level discriminators. A fraction of these events contain a Xenon L-escape photon which is pulse height analyzed. Figure 1 shows an example of the calibration spectrum measured for single lower level discriminator events and (upper trace) all calibration flagged events. Table 1 gives the energies of the lines.

Table 2 gives the mean channel from gaussian fits to the various lines in fig 1 from data obtained 97 Jan 01.

PCARMF (the PCA matrix builder) currently supports two channel to energy conversions: model 2 is a fit to $ch = a + b \times E + c \times E^2$ while model 3 is a fit to $ch = a + b \times E_p + c \times E_p^2$. E_p is defined as $\frac{22 \times E}{w(E)}$ where $w(E)$ is the average energy required to produce one electron in Xenon as a function of photon energy. Fig. 2 plots $w(E)$ vs photon energy; the data comes from the measurements and calculations of [Santos et al. (1991), Santos et al. (1994), Dias et al. (1996)]. Examination of this figure indicates that using E_p naturally includes the energy shifts measured at the atomic edges in Xenon proportional counters [Bavdaz et al. (1995), Tsunemi et al. (1993)] and others.

Fitting either channel to energy relationship is plagued by the fact that the Xe L line is by far the least well determined line, and it occurs in the region where the largest fraction of the cosmically observed photons are. We performed the channel to energy fits in an iterative approach where we shifted the fit Xe L channel by varying amounts, up to 1 channel in the extreme case, and forced the energy to channel fit to go through this point. We selected the offset for each detector by minimizing the residuals of a power-law fit to data from the Crab nebula. To date this iterative procedure has been performed for the first layer of each detector (where most of the photons below 10 keV are detected). Results of the fits to model 2 are given in table 3; results of fits to model 3 are given in table 4.

3 Quantum Efficiency

The quantum efficiency is calculated using photo electric cross sections for Xenon, Propane, Mylar, Aluminum, and Methane. [Henke et al. 1982, Henke et al. 1993, Veigele 1973] An exploded view of a PCU is shown in [Zhang et al. 1994].

The propane, mylar, and aluminum thicknesses are based on nominal densities. The propane layer is 1.3 cm thick and filled to 798 torr at 20°C. The mylar windows are nominally 0.0009 inch thick with a density of 1.4 gm cm⁻³. The nominal aluminum coating is 700 angstroms per side; the bulk density of aluminum is 2.7 gm cm⁻³. At this stage of calibration, we use nominal values for all of these quantities.

Each veto volume is also known to contain Xenon which has permeated from the main volume into the veto volume. This value is determined by fitting, and is sensitive to the other details, particularly the energy to channel relationship for each detector.

The main detector volume is divided into three sensitive xenon layers, of which the front layer is the thickest. The Xenon volume is nominally filled with 840 torr of a 90/10 mixture of Xenon and Methane. The amount of xenon per layer in grams per square cm is an input parameter; we assume that 1 in every 10 molecules is methane, although this has a very small effect on the derived photoelectric efficiency. Compton scattering, which may reduce the efficiency at the higher energies by a small fraction, is not currently included. The efficiency is corrected for a self vetoing term due to the initial photo electron leaving a track in 2 detector cells and therefore being vetoed. The non vetoed fraction is parameterized as $1 - A \times (E/B)^{1.86}$ with default values for A and B of 0.03 and 16 keV. Varying the coefficient A can change the apparent powerlaw index of a continuum source.

Figure 3 shows the relative quantum efficiency for the entire PCA, and the first, second, and third layers. This figure assumes that each detector has a net open area of 1400 cm², a figure which is not yet well calibrated.

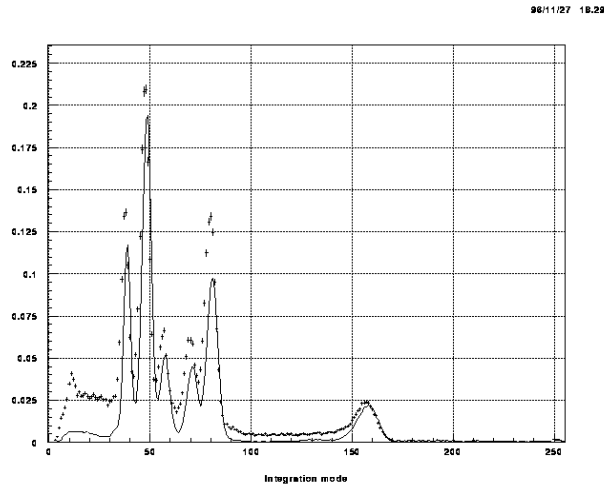


Figure 1: Typical calibration spectra observed with α plus 1 LLD only, and with α plus any combination.

Table 1: Calibration line energies

Line number	Energy (keV)	$\frac{E_\gamma}{w(E)}$	Line source
1	4.110	186.47	Xenon L-escape
2	13.925	637.51	Np L_α
3	17.534	804.40	Np L_{beta}
4	21.125	970.85	Np L_{gamma}
5	~ 26		blend K β escape from 7 and Am^{241}
6	29.870	1372.75	K α escape line from 7
7	59.537	2735.71	Am^{241}

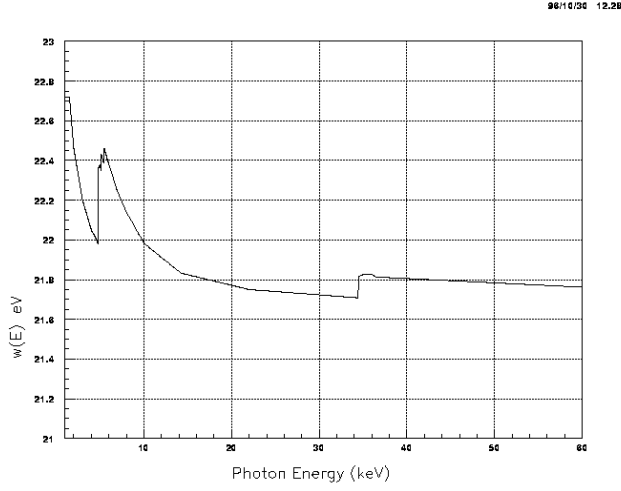


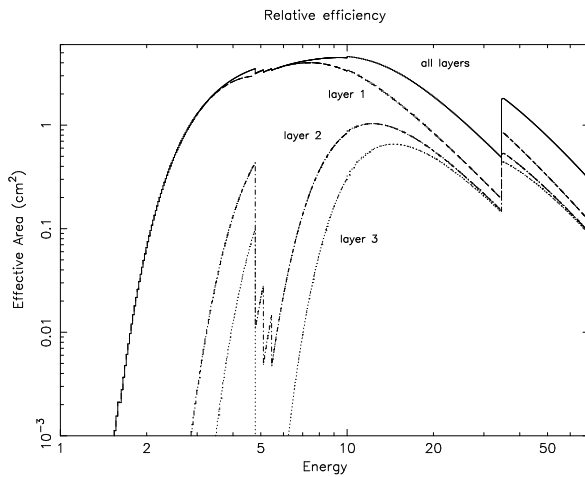
Figure 2: Average energy required to create one electron for photons absorbed in Xenon

Table 2: Fits to epoch 3 calibration lines

Energy	4.110	13.925	17.534	21.125	29.87	59.537
Energy-p	4.102	14.025	17.697	21.359	30.20	60.186
Pcu0 LR1	11.28	38.20	47.98	57.20	80.84	157.49
Pcu0 LR2	10.67	37.79	47.49	56.77	80.04	156.58
Pcu0 LR3	11.43	37.77	47.45	56.64	79.96	156.18
Pcu0 all	11.32	37.85	47.58	56.83	80.27	156.77
Pcu1 LR1	11.12	39.20	49.30	58.75	83.03	162.05
Pcu1 LR2	10.91	39.04	49.09	58.54	82.85	162.13
Pcu1 LR3	11.39	39.81	50.02	59.74	84.34	164.90
Pcu1 all	11.35	39.49	49.56	59.07	83.41	163.04
Pcu2 LR1	10.82	38.03	47.95	57.23	80.91	158.12
Pcu2 LR2	11.03	38.71	48.60	57.94	81.82	160.10
Pcu2 LR3	11.17	37.62	47.26	56.48	79.82	156.15
Pcu2 all	11.15	37.97	47.82	57.13	80.80	158.02
Pcu3 LR1	11.63	40.77	51.33	61.24	86.35	167.90
Pcu3 LR2	11.81	40.83	51.31	61.15	86.29	168.52
Pcu3 LR3	12.09	40.94	51.36	61.25	86.41	168.73
Pcu3 all	12.02	40.88	51.34	61.21	86.35	168.40
Pcu4 LR1	10.89	36.55	45.83	54.49	77.08	150.64
Pcu4 LR2	10.84	36.53	45.85	54.70	77.22	150.96
Pcu4 LR3	10.78	36.26	45.56	54.35	76.63	149.78
Pcu4 all	10.82	36.38	45.71	54.50	76.97	150.46

Table 3: Energy to channel coefficients for Epoch 3, model 2

PCU	lld	model	A	B	C	offset at Xe L
0	3	2	-5.2498E-01	2.7590E+00	-1.9224E-03	-0.5
0	12	2	-1.1701E+00	2.7686E+00	-2.1931E-03	
0	48	2	-1.6226E-01	2.7053E+00	-1.4718E-03	
0	63	2	-1.6226E-01	2.7053E+00	-1.4718E-03	
1	3	2	-6.4282E-01	2.8337E+00	-1.8801E-03	-0.15
1	12	2	-8.5773E-01	2.8346E+00	-1.8130E-03	
1	48	2	-3.8865E-01	2.8351E+00	-1.2473E-03	
1	63	2	-6.1887E-01	2.8855E+00	-2.3526E-03	
2	3	2	-7.2808E-01	2.7690E+00	-1.8411E-03	-0.2
2	12	2	-5.9699E-01	2.7876E+00	-1.6793E-03	
2	48	2	-1.5234E-01	2.7126E+00	-1.5314E-03	
2	63	2	-4.3909E-01	2.7793E+00	-1.9854E-03	
3	3	2	-3.0877E-01	2.9380E+00	-2.0498E-03	+0.1
3	12	2	1.6548E-02	2.8998E+00	-1.3581E-03	
3	48	2	3.9377E-01	2.8747E+00	-9.8965E-04	
3	63	2	2.8547E-02	2.9507E+00	-2.0863E-03	
4	3	2	-5.3055E-01	2.6279E+00	-1.6713E-03	-0.65
4	12	2	-6.2904E-01	2.6400E+00	-1.7484E-03	
4	48	2	-5.8501E-01	2.6145E+00	-1.6838E-03	
4	63	2	-7.9539E-01	2.6778E+00	-2.3553E-03	



kelth 8-Jan-1997 13:01

Figure 3: Relative efficiency for the total PCA and the sum of the individual layers

Table 4: Energy to channel coefficients for Epoch 3, model 3

PCU	lld	model	A	B	C	offset at Xe L
0	3	3	-2.3636E-01	2.6660E+00	-8.0509E-04	-0.6
0	12	3	-8.8131E-01	2.6757E+00	-1.0705E-03	
0	48	3	1.2015E-01	2.6138E+00	-3.7821E-04	
0	63	3	1.2015E-01	2.6138E+00	-3.7821E-04	
1	3	3	-3.4250E-01	2.7380E+00	-7.3206E-04	-0.25
1	12	3	-5.5692E-01	2.7388E+00	-6.6083E-04	
1	48	3	-8.7428E-02	2.7392E+00	-1.0780E-04	
1	63	3	-2.7680E-01	2.7791E+00	-1.0569E-03	
2	3	3	-4.3691E-01	2.6755E+00	-7.1738E-04	-0.3
2	12	3	-3.0316E-01	2.6935E+00	-5.5325E-04	
2	48	3	1.3293E-01	2.6205E+00	-4.2878E-04	
2	63	3	-1.1195E-01	2.6765E+00	-7.3811E-04	
3	3	3	7.3369E-03	2.8385E+00	-8.5491E-04	-0.0
3	12	3	3.2875E-01	2.8013E+00	-1.8278E-04	
3	48	3	7.0312E-01	2.7768E+00	1.6856E-04	
3	63	3	3.8302E-01	2.8412E+00	-7.5750E-04	
4	3	3	-2.6167E-01	2.5398E+00	-6.1425E-04	-0.75
4	12	3	-3.5816E-01	2.5514E+00	-6.8563E-04	
4	48	3	-3.1867E-01	2.5269E+00	-6.3386E-04	
4	63	3	-4.8801E-01	2.5799E+00	-1.1607E-03	

The default values for parameters which affect the quantum efficiency estimate are

(xe_gm_cm2_l1_p0 = 0.00750)	Enter gm/cm ² Xe in layer 1
(xe_gm_cm2_l2_p0 = 0.0060)	Enter gm/cm ² Xe in layer 2
(xe_gm_cm2_l3_p0 = 0.0060)	Enter gm/cm ² Xe in layer 3
(xe_gm_cm2_pr0 = 2.3e-04)	Enter gm/cm ² Xe in propane layer
(xe_gm_cm2_l1_p1 = 0.00750)	Enter gm/cm ² Xe in layer 1
(xe_gm_cm2_l2_p1 = 0.0060)	Enter gm/cm ² Xe in layer 2
(xe_gm_cm2_l3_p1 = 0.0060)	Enter gm/cm ² Xe in layer 3
(xe_gm_cm2_pr1 = 2.2e-04)	Enter gm/cm ² Xe in propane layer
(xe_gm_cm2_l1_p2 = 0.00750)	Enter gm/cm ² Xe in layer 1
(xe_gm_cm2_l2_p2 = 0.00600)	Enter gm/cm ² Xe in layer 2
(xe_gm_cm2_l3_p2 = 0.00600)	Enter gm/cm ² Xe in layer 3
(xe_gm_cm2_pr2 = 2.0e-04)	Enter gm/cm ² Xe in propane layer
(xe_gm_cm2_l1_p3 = 0.00750)	Enter gm/cm ² Xe in layer 1
(xe_gm_cm2_l2_p3 = 0.0060)	Enter gm/cm ² Xe in layer 2
(xe_gm_cm2_l3_p3 = 0.0060)	Enter gm/cm ² Xe in layer 3
(xe_gm_cm2_pr3 = 1.8e-04)	Enter gm/cm ² Xe in propane layer
(xe_gm_cm2_l1_p4 = 0.00750)	Enter gm/cm ² Xe in layer 1
(xe_gm_cm2_l2_p4 = 0.0060)	Enter gm/cm ² Xe in layer 2
(xe_gm_cm2_l3_p4 = 0.0060)	Enter gm/cm ² Xe in layer 3
(xe_gm_cm2_pr4 = 2.8e-04)	Enter gm/cm ² Xe in propane layer
(pr_gmcm2 = 0.00261)	Enter gm/cm ² in Propane layer
(my_gmcm2 = 0.00708)	Enter gm/cm ² of (summed) Mylar windows
(al_gmcm2 = 7.6e-5)	Enter gm/cm ² of (summed) Aluminum
(epoint = 16.0)	Enter reference energy for electron tracks
(track_coeff = 0.01)	Enter coefficient for electron tracks

4 Response to Monochromatic input

The PCA response is non diagonal, with the most important effects being the finite resolution and the presence of escape peaks. The resolution is modelled as a second order polynomial. The resolution is approximated, for all detectors and all layers as $\sigma = 0.39 + 0.019 \times E + 9.0 \times E^2$ where σ is the FWHM and the coefficients assume that E is measured in keV. The resolution is translated to channels by multiplying by the slope of the energy to channel conversion (B in tables 3 and 4).

Escape peaks are included for all photon energies above the K and L edges; the apparent energy deposited in the counter is slightly different than expected by differencing the incident energy and the energy of the escape photon. The detailed atomic physics has been modelled by [Dias et al. (1996)] and we parameterize this as a change in the number of electrons produced in the gas compared to the naive expectation (which can be translated to eV by multiplying by $w(E)$). We parameterize the non trivial chance that a detected photon above the K edge will be vetoed through detection of the escape photon in another layer of the detector. This parameter is highly coupled to the Escape Fractions, since both parameters can change the estimate of how many photons are observed above the edge in a direct way. The escape fraction causes the matrix to predict that some of these photons are observed at different energies; the self veto fraction simply removes these photons altogether.

The assumed escape fractions and energy offsets for the escape peaks are parameterized as follows:

```
(EscFracKb = 0.155)      Enter fraction of K-beta  escape
(EscFracKa = 0.545)      Enter fraction of K-alpha escape
(EscFracL1 = 0.010)      Enter fraction of L-alpha escape, 1st layer
(EscFracL2 = 0.000)      Enter fraction of L-alpha escape, 2nd layer
(EscFracL3 = 0.000)      Enter fraction of L-alpha escape, 3rd layer
(EscFracLt = 0.009)      Enter fraction of L-alpha escape, detect. ave.

(delta_el_L = 3.9)       electron offset for L escape
(delta_el_Ka = -2.26)    electron offset for K-alpha escape
(delta_el_Kb = 3.84)     electron offset for K-beta escape

(xe_kedge_veto = 0.85)   Enter non-self veto frac above K-edge
```

Figure 4 shows the response to 2 zero width gaussians at 8 and 55 keV. The L escape peak from the lower line and the 2 K escape peaks from the higher line are clearly visible. L escapes are not included for lines above the K edge; the fraction is small and is blended with the main peak. Other partial charge collection effects, such as a tail on the low energy side of any of the peaks are not currently included.

5 RESULTS

We show three fits to Crab Spectra, designated `case1` which uses energy to channel conversion model 3 and PCARMF v2.1; `case2` which uses energy to channel conversion modle 2 and PCARMF v2.02 (part of ftools release 3.6.1); and `case_2pob` which fits the Crab as a sum of two power laws using the same matrices as `case 1`. The derived parameters for `case1_2pob` vary widely from detector to detector and require additional constraints. We fix the slope of the second power law (associated with the pulsed component) at 1.73 [Pravdo and Serlemitsos 1981]. We plan to fix the parameters of the harder power law using PCA data once we have fit the spectrum of the pulsed component. The two power law fit is motivated by the well known observation that the pulsed component of the Crab is harder than the unpulsed component.

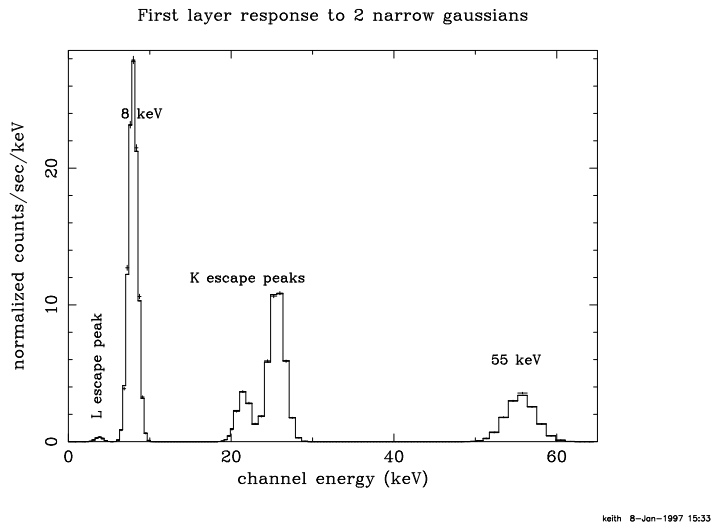


Figure 4: First layer response to two narrow gaussians

Table 5: Summary of case 1, v2.1, model 3

data	Γ	Norm	χ^2_ν
p0lr1	2.05	10.1	10.5
p1lr1	2.09	11.0	14.1
p2lr1	2.05	10.2	9.8
p3lr1	2.05	9.9	15.0
p4lr1	2.06	10.1	9.8
p0all	2.08	10.8	9.2
p1all	2.11	11.7	17.9
p2all	2.08	10.9	10.5
p3all	2.08	10.6	11.6
p4all	2.09	10.8	12.0
5 first layers	2.06	10.2	12.8
5 PCU	2.09	10.9	13.3
full PCA	2.09	10.9	55.3

Table 6: Summary of case 2, v2.02, model 2

data	Γ	Norm	χ^2_ν
p0lr1	2.06	8.9	5.7
p1lr1	2.14	10.3	15.0
p2lr1	2.08	9.2	6.7
p3lr1	2.06	8.7	7.4
p4lr1	2.11	9.4	4.0
p0all	2.06	9.2	6.0
p1all	2.17	11.3	83.7
p2all	2.07	9.04	6.6
p3all	2.07	9.3	10.0
p4all	2.10	9.7	10.8
5 first layers	2.09	9.3	13.0
5 PCU	2.09	9.7	35.9
full PCA	2.09	9.7	43.4

Table 7: summary of case 1 - 2 power laws, 2nd $\Gamma = 1.73$

data	$\Gamma 1$	Norm1	χ^2_ν
p0lr1	2.23	9.0	8.6
p1lr1	2.28	10.2	11.5
p2lr1	2.24	9.1	7.6
p3lr1	2.43	9.2	8.0
p4lr1	2.18	9.3	9.0
p0all	2.21	10.1	7.3
p1all	2.32	11.3	12.3
p2all	2.25	10.2	7.3
p3all	2.34	10.0	5.5
p4all	2.23	10.1	9.9
5 first layers	2.26	9.2	10.3
5 PCU	2.27	10.3	9.7
full PCA	2.26	10.2	39.2

References

- [Bavdaz et al. (1995)] Bavdaz, M., Martin, D., and Peacock, A. 1995, SPIE 2518, ppp.
- [Dias et al. (1996)] Dias, T.H.V.T et al., 1996, IEEE-Trans. Nucl. Sci, in press.
- [Henke et al. 1982] Henke, B.L., Lee, P., Tanaka, T. J., Shimabukuro, R. L., and Fujikawa, B. K. 1982, Atomic Data and Nuclear Data Tables, 27, 1.
- [Henke et al. 1993] Henke, B. L., Gullikson, E. M., and Davis, J. C., 1993, Atomic Data and Nuclear Data Tables, 54, 181; http://www-cxro.lbl.gov:80/optical_constants/
- [Jahoda et al. (1996)] Jahoda, K., Swank, J. H., Giles, A. B., Stark, M. J., Strohmayer, T., Zhang, W., and Morgan, E. H., 1996, SPIE 2808, 59.
- [X-ray Data Booklet] Kirz, J. et al., "X-ray Data Booklet", Center for X-ray Optics, Lawrence Berkeley Laboratory, 1986.
- [Pravdo and Serleimitsos 1981] Pravdo, S. H. and Sereleimitsos, P. J. 1981, Astrophysical Journal, 246, 484.
- [Santos et al. (1991)] Santos, F.P., Dias, T.H.V.T., Stauffer, A.D., and Conde, C.A.N. 1991, Nuclear Instruments and Methods, A307, 347.
- [Santos et al. (1994)] Santos, J.M.F., Morgando, R.E., Tavora, L.M.N., and Conde, C.A.N., 1994, Nuclear Instruments and Methods, A350, 216.
- [Tsunemi et al. (1993)] Tsunemi, H., Hayashida, K., Torri, K., Tamura, K., Miyata, E., Murakami, H., and Ueno, S., 1993, Nuclear Instruments and Methods, A336, 301.
- [Veigele 1973] Veigele, W. J. 1973, Atomic Data Tables, 5, 51.
- [Zhang et al. 1994] Zhang, W., Giles, A. B., Jahoda, K., Soong, Y., Swank, J. H., and Morgan, E. H. 1994, SPIE 2006, 324.